# Phosphetene-based polyaromatics: structure-property relationships and chiroptical tuning

Hortense Lauwick, Erik Kertész, Kristóf Noel Garami, Wimonsiri Huadsai, Matthew Duffy, Roukayaati Foundi, Alexandre Chemin, Thierry Roisnel, Nicolas Vanthuyne, Zoltán Benkő, et al.

How to cite: *Angew. Chem. Int. Ed.* **2024**, *63*, e202409988
doi.org/10.1002/anie.202409988

Chiral Organic Emitters

# Phosphetene-Based Polyaromatics: Structure-Property Relationships and Chiroptical Tuning

*Hortense Lauwick, Erik Kertész, Kristóf Noel Garami, Wimonsiri Huadsai, Matthew P. Duffy, Roukayaati Foundi, Alexandre Chemin, Thierry Roisnel, Nicolas Vanthuyne, Zoltán Benkő,* Pierre-Antoine Bouit,* and Muriel Hissler**

**Abstract:** We describe the synthesis of π-extended phosphetene rings (4-member P-rings) flanked with PAH systems of various topologies. These compounds are fully characterized including X-ray diffraction. The impact of both the polyaromatic platform and the P-ring on the structure, and the optical and redox properties are investigated both experimentally and theoretically. Although neither the P centre nor the 4-membered ring significantly takes part in the HOMO or LUMO orbitals, both structural features have an important modulating role in distorting the symmetry of the orbitals, leading to chiroptical properties. The stereogenic P-atom is used as a remote chiral perturbator to induce circularly polarized luminescence of the polyaromatic system. The dissymmetry factor is highly dependent on the polyaromatic topology, as supported by theoretical calculations.

**P**olycyclic Aromatic Hydrocarbons (PAHs) are π-conjugated systems consisting of fused aromatic rings that find many applications in the field of optoelectronics.[1] Their properties are mainly defined by their fusion patterns at the molecular level. For example, linearly fused systems display high charge carrier mobility and thus have been widely used as p-semiconductors in Organic Field-Effect Transistors (OFETs).[1] When the rings are angularly arranged, the compounds display a helical π-framework which is configurationally stable depending on the number of ortho-fused rings and their substituents. Such compounds, called helicenes (for example [6]helicene **A**, Figure 1) show excellent chiroptical properties due to the inherent chirality of the π-framework: e.g. optical rotation, circular dichroism and circularly polarized luminescence (CPL) with luminescence dissymmetry factor ($g_{lum}$) values up to $10^{-2}$ for substituted [6]helicenes.[2] As an example of applications, [6]helicenes were used to design circularly polarized organic light-emitting diodes (CP-OLEDs).[3] An elegant alternative strategy for designing CP-emitters is to prepare a chirally perturbated fluorophore.[4] In such a derivative, a chiral centre is located in the vicinity of an achiral emitter, inducing its chiroptical properties. BINOL substituted-BODIPY **B** (Figure 1) is a representative example of this emerging class of CP-emitters that also found application in OLEDs.

In this work, we aimed to use the chiral perturbation of a stereogenic P-atom (within a phosphetene ring) to chirally perturb PAH-based π-systems. Hence, phosphetene is a 4-membered P-ring that, despite being barely investigated,[5] has started to be used in the context of molecular materials and optoelectronics.[6] We describe the synthesis of eight new π-extended phosphetene rings flanked with PAH systems of various topologies (Figure 1). The impact of both the polyaromatic system and the P-ring on the structure, as

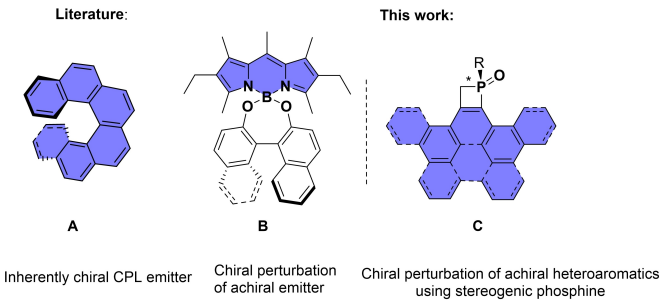


***Figure 1.*** Examples of CPL emitters (**A**–**B**) and compound studied in this work (**C**) (blue part represents the fluorophore in each molecule).

[*] Dr. H. Lauwick, W. Huadsai, Dr. M. P. Duffy, R. Foundi, A. Chemin, T. Roisnel, Dr. P.-A. Bouit, Prof. M. Hissler
Univ Rennes, CNRS, ISCR – UMR 6226
F-35000 Rennes
E-mail: pierre-antoine.bouit@univ-rennes.fr
muriel.hissler@univ-rennes.fr

E. Kertész, K. N. Garami, Prof. Z. Benkő
Department of Inorganic and Analytical Chemistry
Budapest University of Technology and Economics
Műegyetem rkp. 3, H-1111 Budapest
E-mail: benko.zoltan@vbk.bme.hu

Prof. Z. Benkő
HUN-REN-BME Computation Driven Chemistry Research Group,
1111 Budapest, Műegyetem rkp. 3, Hungary

Dr. N. Vanthuyne
Aix Marseille Univ., CNRS, Centrale Marseille, FSCM, Chiropole
13397 Marseille Cedex 20, France

well as the optical and redox properties of the compounds are investigated experimentally and using theoretical methods. Finally, we show that the stereogenic P-ring acts as an efficient chiral perturbator to induce circularly polarized luminescence of the polyaromatic system with $g_{lum}$ of $\sim 10^{-3}$. The dissymmetry factor is highly dependent on the polyaromatic topology.

To prepare phosphetenes **1–4**, Doxsee's one-pot methodology was used starting from the corresponding alkynes (Scheme 1).[7] The phosphetenes having trivalent P-centres ($^{31}$P NMR: ~−17 ppm) were oxidized *in situ* to form the corresponding phosphetene oxides ($^{31}$P NMR: ~+20 ppm), which can easily be handled in air. All compounds were synthesized in moderate yields (31–46 %) and were fully characterized by multinuclear NMR and mass spectrometry and their structures were unequivocally confirmed by single crystal X-ray diffraction (Scheme 1 and ESI). The unit cells are all composed of a racemic mixture of the two enantiomers, with the P atom as a stereogenic centre. In all these derivatives, the P-ring is a distorted square (Table S2) with usual bond lengths and angles for phosphetenes.[6] The lateral aryl groups are twisted from the plane of the P-ring. Such a structural property will have an impact on the conjugation in the systems (see below). No intermolecular interactions were observed in the packing.

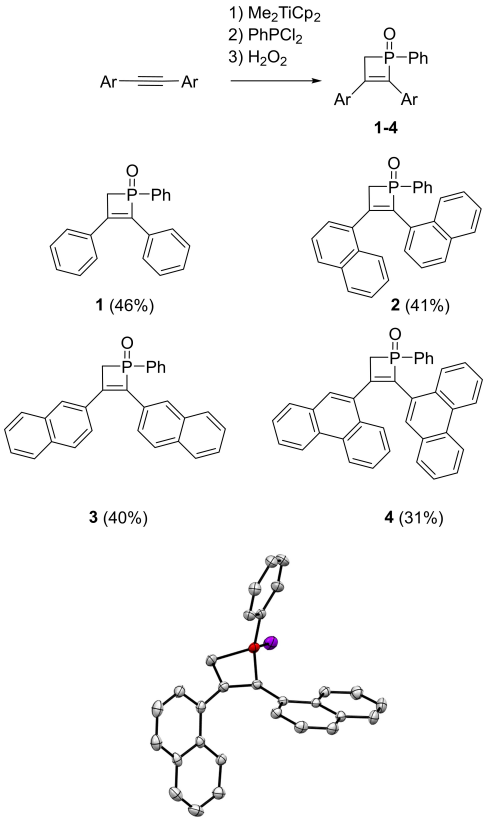


***Scheme 1.*** Synthesis route to **1–4** (up) and X-ray structures of **2**. Hydrogen atoms are omitted for clarity and thermal ellipsoids are set at 50 % probability.

The optical (absorption/emission) properties of compounds **1–4** were investigated in diluted DCM solutions ($c = 5 \cdot 10^{-6}$ mol·L$^{-1}$, Figure 2 and Table S4). Stilbene analogues **1–4** display large UV/Vis absorption bands in the visible range. As expected, the extension of the π-skeleton leads to a bathochromic/hyperchromic shifts. All derivatives are also luminescent in diluted solution and show broad and unstructured emission in the blue region with good quantum yields ($0.2 < \phi < 0.5$) except for **1** ($\phi = 0.02$). These emissions display large Stokes-shifts~6800–12000 cm$^{-1}$ and a lifetime in the range of the ns (Table S5).

To understand the nature of the electronic excitations TD-DFT (time-dependent density functional theory, using the B3LYP and ωB97X-D functionals) and ADC(2) (second order algebraic-diagrammatic construction) calculations were performed. Due to the rotation of the aryl groups several conformers may coexist in solution, which have rather similar energies, as outlined by DFT calculations. These rotamers have only slightly different absorption wavelengths and the TD-DFT and higher level ADC(2) calculations lead to the same conclusions. On the basis of these calculations, the first excitations can be attributed to practically pure HOMO–LUMO transitions of π–π* character (Figure 3 and Table S6). Additionally, the principle natural transition orbitals (pNTOs, see Figure S38) obtained from ADC(2) calculations are highly similar to the Kohn–Sham orbitals.

In general, both FMOs of **1–4** are mainly delocalized over the C=C bond of the P-ring and the π-systems of its

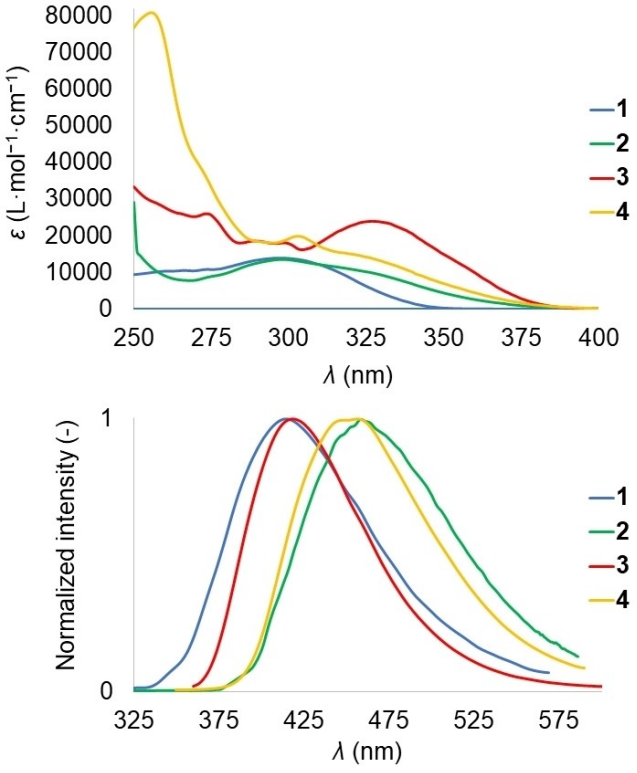


***Figure 2.*** UV/Vis absorption (up) and normalized emission spectra (down) of **1–4** in DCM ($c = 10^{-6}$ M).

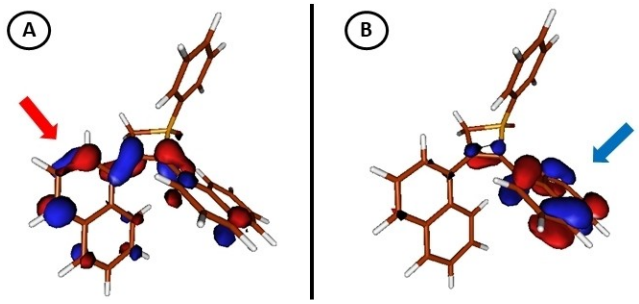


***Figure 3.*** Kohn–Sham FMOs of ***(R)*-2**, (A): LUMO, (B): HOMO (isosurface value of 0.05, calculations at the TD-B3LYP-D3/6-31G*//B3LYP-D3/6-31G* level of theory).

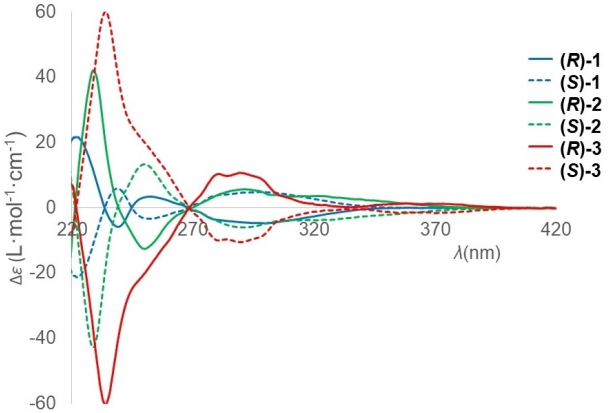


***Figure 4.*** ECD spectra of the enantiomers (**R/S**) **1–3** in DCM ($c = 10^{-5}$ M).

substituents (similar to *Z*-stilbene, Figure S39). According to the Mulliken partition analysis (MPA) of these orbitals, the parts of the phosphetene units without the olefinic carbon atoms have negligible contributions (remarkably, the P centre is below 3 % in all the cases, Table S7). Regarding specifically the C=C unit in the phosphetene ring in **1–4**, the lobes of the orbitals are strongly dissymmetric (regarding the quasi plane of the phosphetene ring and also perpendicular to it). Similar dissymmetry can be observed on the lateral π-substituents as well. The MPA allowed us to conclude that, in general, the HOMOs have significantly higher contributions at the substituents being proximal to the stereogenic P centre (Figure 3, blue arrow), while the LUMOs spread over the distal substituents (Figure 3, red arrow). These results already prognose the possibility of chiroptical properties, which will be presented below.

The TD-DFT calculations are able to reproduce properly the experimental Stokes-shifts, which can be explained by the substantial rotation of the lateral π-substituents at the excited state (Figure S40 and Table S8).

As mentioned above, the P-atom in these systems is stereogenic. To investigate the effect of the chirality on the optical properties, enantiopure samples (with ee > 99.5 %) of derivatives **1–3** were obtained via HPLC using a chiral stationary phase (see ESI).[8] Electronic circular dichroism (ECD) was recorded in diluted DCM solutions. All pairs of enantiomers displayed ECD with the expected mirror-image relationship (Figure 4). For example, ***(R)*-2** shows various positive ($\Delta\varepsilon = +42$ at 229 nm, $\Delta\varepsilon = +6$ at 292 nm), and negative bands ($\Delta\varepsilon = -13$ at 250 nm). However, no general pattern can be observed regarding the alternation of positive/negative bands in this family. Nevertheless, the results of TD-DFT and ADC(2) calculations are consistent with the experiments (the patterns and relative intensities are similar and the wavelengths deviate by ±20 nm, see Table S8–9 Figure S41–S76). Therefore, assignment of the absolute configurations in the experimental ECD spectra could be obtained using comparison with the analogous spectra computed at the ADC(2) level. For the most red-shifted transition, the absorption dissymmetry factor $g_{abs}$(**2**) is $5 \cdot 10^{-4}$ at 290 nm, and the other derivatives also present dissymmetry factors in the same order of magnitude. The CPL properties were also studied. While **1**, which displays a very small luminescence quantum yield (Table S4), did not show any detectable CPL, moderate to weak CPL were detected for **2** ($g_{lum} \sim 7 \cdot 10^{-4}$ at 410 nm) and **3** ($g_{lum} \sim 3 \cdot 10^{-4}$ at 410 nm) (Figure S36), close to the limit of detection of our setup. These values agree with the dissymmetry factors measured in ECD (Figure S35).[9] The $g_{lum}$ values for **2–3** are in the lower range of organic CPL emitters,[2] which however nicely illustrates the chiral perturbation induced by the presence of the remote stereogenic P-atom.[10]

The molecular structures of **1–4**, exhibiting heterocycle-substituted stilbene backbones make them ideal synthons to promote photoinduced intramolecular cyclization. Indeed, the reaction of **1** and **2** in the "Katz" conditions (hν, $I_2$, propylene oxide)[11] leads to the formation of phenanthrene-(**5**, Scheme 2) and picene-substituted phosphetene oxides (**6**, Scheme 2) in good yields (70–72 %). In the case of **3–4**, the reaction does not stop after the first cyclization, and a second cyclization occurs to yield planar PAH-substituted phosphetenes **7** and **8** (74 %–83 %).[12] All the derivatives were fully characterized by multinuclear NMR, mass spectrometry and the structures of **5** and **6** were further confirmed by single crystal X-ray diffraction (Scheme 2). Again, the structures consist of a racemic mixture of enantiomers, and the geometry of the P-ring is not significantly altered by the cyclization. In these systems, the polyaromatic scaffold is mostly planar (maximal deviation from the mean polyaromatic plane in **6**: 0.14 Å). No intermolecular interactions based on π-stacking of the PAH framework can be observed in the packing.

The presence of an electron-withdrawing P=O impacts the redox properties. Compared to the pure hydrocarbon analogs, the cyclic voltammetry measurements revealed that **6–8** display monoelectronic quasi-reversible reduction waves at moderated potential ($E_{red} \sim -2.2$ V vs Fc, see Table S4 and Figure S37). This redox behaviour arises from the presence of the electron-deficient phosphine oxide moiety directly attached to the PAH backbone.[13]

The optical (absorption/emission) properties of **5–8** have also been investigated in diluted DCM solutions ($c = 5 \cdot 10^{-6}$ mol·L$^{-1}$, Figure 5 and Table S4). The UV/Vis absorption spectra of **5–8** are in marked contrast with those of their

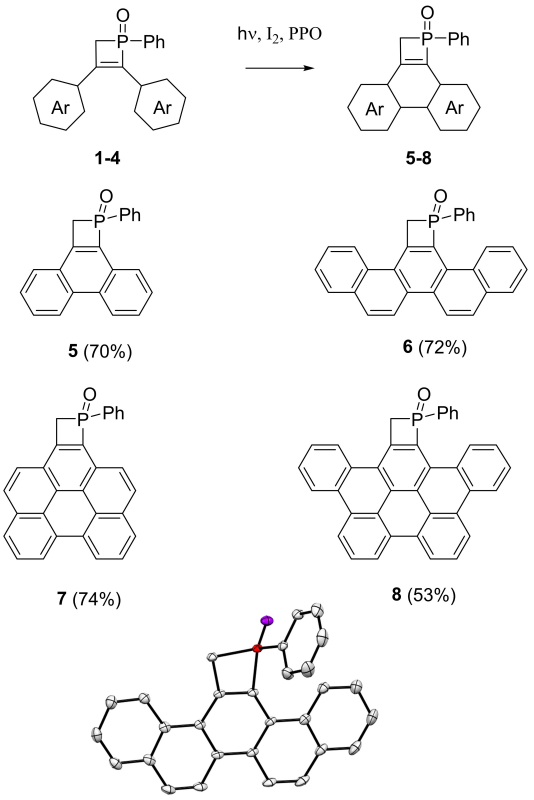


***Scheme 2.*** Synthesis route to **5–8** (up) and X-ray structures of **6**. Hydrogen atoms are omitted for clarity, and thermal ellipsoids are set at 50% probability.

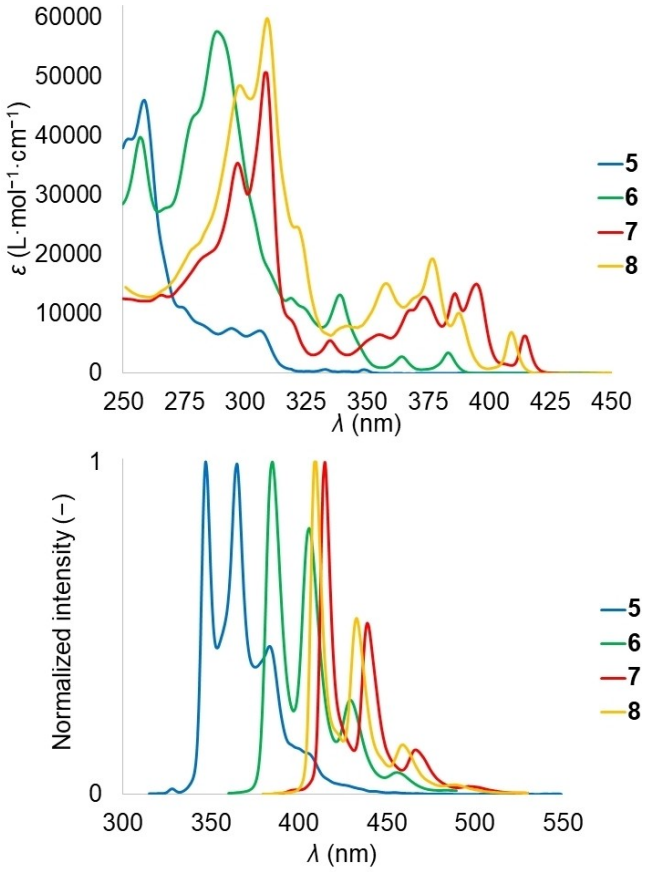


***Figure 5.*** UV/Vis absorption (up) and normalized emission spectra (down) of **5–8** in DCM ($c = 10^{-6}$ M).

precursors **1–4**. Indeed, they all display finely structured absorption bands in the 300–440 nm range, characteristic for PAHs derivatives (Figure 5). The effect of the P-ring on the absorption is limited compared to the purely hydrocarbon analogues.[14] In general, the difference between the absorption wavelengths of compounds **5–8** and their corresponding parent PAH is ~10 nm and the largest deviation was found for compound **5**, displaying a redshift of 19 nm compared to phenanthrene (Table S15). As expected, the extension of the π-backbone in the series **5–6–7** leads to gradual bathochromic shifts and the highest absorption wavelength is reached for the benzo[*g,h,i*]perylene analogue **7** at 415 nm. However, further extension of the π-system resulting in PAH **8** ($\lambda_{max} = 409$ nm) affords a slight blueshift compared to **7**. In general, significant bathochromic shifts (51–88 nm) can be observed compared to their corresponding starting materials **1–4**.

As TD-DFT calculations could not properly simulate the excited states of **6–8** (Table S8), ACD(2) calculations were applied, which not only predict a correct pattern, but also offer acceptable quantitative agreement for the **5–8** series. Based on these data, the sets of low energy/low intensities peaks for **5–8** belong to the vibrational fine structures of the lowest energy excitations. The wavenumbers corresponding to these vibrational transitions are rather similar for the four compounds encompassing a narrow range between 1220 and 1390 $cm^{-1}$, being consistent with the typical calculated span of 1200–1600 $cm^{-1}$ (Table S15). Based on our harmonic vibrational analysis, these transitions may be associated with C–C stretch and C–H bending modes of the aromatic system. The pNTOs corresponding to these excitations show high similarity to the Kohn–Sham orbitals, see Figure 6. Therefore, the low energy transition, assigned to $^1L_b$ (employing Platt's nomenclature) is a mixture of HOMO-1→LUMO and HOMO→LUMO+1 transitions, while the transition at higher energy ($^1L_a$) can be described as a pure HOMO→LUMO transition.[15] According to MPA, again the P-atom is again practically not involved in any of these transitions, and the optical properties are mainly determined by the PAH cores.

The emission spectra of **1–4** also strongly differ from their precursors because finely structured emission bands with very low Stokes shifts are observed (Figure 5 and Table S4). The lifetime is one order of magnitude higher compared to their precursors (~10 ns, Table S5), but remain in the range of purely fluorescent compounds. The luminescence properties are again highly similar to those of the purely hydrocarbonated analogs.[14] The trend in emission wavelengths in the series agrees with that observed in absorption. These compounds all display high quantum yields ($0.35 < \phi < 0.6$, Table S4), being consistent with their rigid structures.

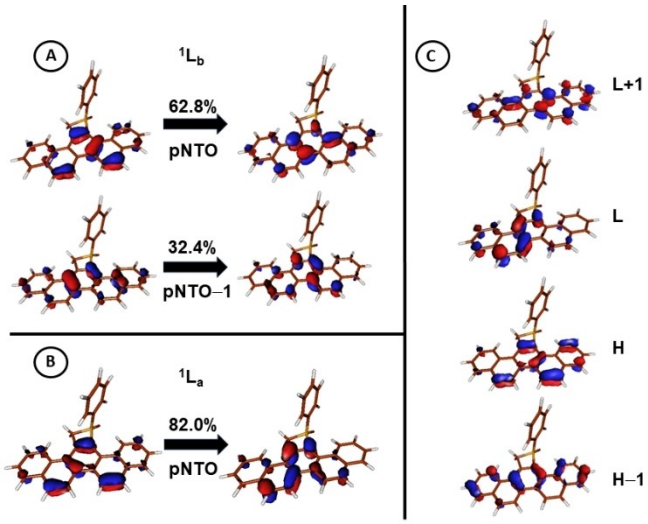


***Figure 6.*** pNTO contributions for the first (A) and second excitation (B) with their weights (above the arrow, ADC(2)/cc-pVDZ//B3LYP-D3/6-31G*) and Kohn–Sham FMOs (C) of ***(R)*-6** (H: HOMO, L: LUMO, isosurface value of 0.05, B3LYP-D3/6-31G*//B3LYP-D3/6-31G*).

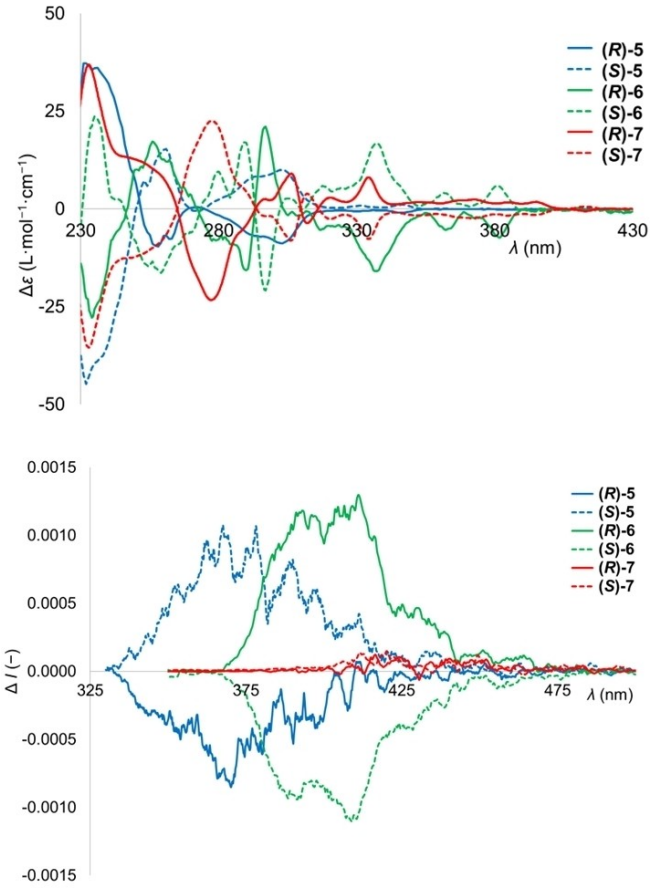


***Figure 7.*** ECD spectra (up) and CPL spectra (down) of (**R**/**S**) **5–7** in DCM ($c = 10^{-5}$ M).

Importantly, four new phosphetene-substituted PAHs (either linear (**5–6**) or extended planar (**7–8**) were prepared, and these compounds demonstrate intense emission in solution characteristic of PAH derivatives.

To investigate the effect of the chirality on the optical properties of fused derivatives **5–7**, enantiopure samples (with ee $>99.5\,\%$) were obtained via HPLC using a chiral stationary phase (see ESI).[8] Electronic circular dichroism was recorded in diluted DCM solutions. All enantiomer pairs display ECD with the expected mirror-image relationship (Figure 7). For example, (***R***)-**6** shows various positive ECD bands ($\Delta\varepsilon = +17$ at 256 nm, $\Delta\varepsilon = +21$ at 297 nm), negative bands ($\Delta\varepsilon = -16$ at 290 nm, $\Delta\varepsilon = -16$ at 337 nm and $\Delta\varepsilon = -7$ at 381 nm). Importantly, the vibrational fine structures are also present in the ECD spectra. As another interesting aspect, the planarization of the system upon cyclization leading to **5–7** induces the appearance of various Cotton effects (see Figure 7 and Figure S44). Within the fused series, while **5** and **6** display a similar alternation of ECD bands (negative/positive/negative/positive/negative) for both (***S***)-**5** and (***S***)-**6**, the ECD spectrum of **7** is completely different, illustrating that the chiroptical response of this latter is significantly distinct from the two preceding ones. Additionally, **7** exhibits higher extinction coefficients and weaker ECD responses in the low energy region, resulting in dissymmetry factors one order of magnitude lower ($g_{abs}(\mathbf{5}) = 2\cdot10^{-3}$ at 345 nm, $g_{abs}(\mathbf{6}) = 1\cdot10^{-3}$ at 384 nm and $g_{abs}(\mathbf{7}) = 6\cdot10^{-5}$ at 410 nm) (see Figure S35).

To decipher the mechanism of chiroptical properties evolution upon extending the π-system, further investigation were performed at the ADC(2) level. The $g_{abs}$ values can be successfully estimated by its theoretical counterpart, $g_{cal}$ (for details see Table S18), which shows the same trend and order of magnitude ($g_{cal}(\mathbf{5}) = 4\cdot10^{-3}$, $g_{cal}(\mathbf{6}) = 2\cdot10^{-3}$ and $g_{cal}(\mathbf{7}) = 1\cdot10^{-4}$) as the experimental values. This observation suggests that the source of chirality is rooted in the molecular orbitals. Indeed, the dissymmetry arising from the perturbation of the chiral phosphetene moiety can be clearly seen on the FMOs and pNTOs (Figure 3 and 6). To quantify the extent of dissymmetry in the orbitals for compounds **5–8**, we employed an orbital dissymmetry factor ($g_{orb}$), which is obtained by averaging the differences in the atomic contribution to each FMO from MPA.[16] Importantly, this $g_{orb}$ factor qualitatively describes the trend of the absorption dissymmetry factors.

To decipher whether the dissymmetry in the orbitals arises from the curvature or nonplanarity of the PAH backbone, the geometries of compounds **5–7** were optimized constraining the PAH backbone in a plane. The ADC(2) calculations on these artificial structures resulted in highly similar ECD spectra to the original counterparts (Figure S77). Furthermore, the very small deviations of the PAH backbones from planarity (typically below 1°, Table S16) also fail to explain the orbital dissymmetry. To measure the bond lengths distortion, we introduce a dimensionless geometry dissymmetry factor ($g_{geom}$), which is based on the differences in the bond lengths on the two sides of the quasi-symmetric PAH core. Importantly, $g_{geom}$ follows the trend of both $g_{orb}$ and $g_{abs}$, and therefore the propagation of chirality can be traced back to the slightly

changing bond lengths. To understand the chirality evolution throughout the ring systems, we also obtained the incremental bond dissymmetries as the differences between the bond lengths of the symmetrically arranged bonds in compounds **5–7** (the average of these values for each of the ring, see Figure 8 and Supporting Information for details). The largest dissymmetry is observed at the six-membered ring attached directly to the phosphetene moiety and the distortion declines with the distance along the neighbouring rings from the center of chirality towards the periphery of the molecule. In general, the more aromatic rings (lower NICS(0) values, blue in Figure 8) that can be termed as Clar aromatic (indicated by white circles in Figure 8) allow lower degrees of distortion. Due to these differing distortion increments, the transfer of chirality is more effective for compound **6** having a zigzag array of aromatic rings compared to **7** with a more rigid and compact structure. Indeed, the lateral expansion of the chain from PAH **5** to **6** does not alter significantly the $g_{abs}$ value, while the medial extension in two dimensions from **5** to **7** results in a significant decrease in the dissymmetry factor (in $g_{abs} = 2 \cdot 10^{-3}$ and $6 \cdot 10^{-5}$ for **5** and **7**, respectively). These results outline that the effect of chiral perturbation depends on the cross connections and rigidity of PAH structures.

Interestingly, **5** and **6** present quite remarkable CPL (Figure 7) with $g_{lum} \sim 9 \cdot 10^{-4}$ at 370 nm for **5** and $g_{lum} \sim 1.1 \cdot 10^{-3}$ at 408 nm for **6**, while the CPL of **7** is barely detectable ($g_{lum} \sim 1 \cdot 10^{-4}$, which falls again in the detection limit of our setup). Remarkably, this is in good agreement with their respective $g_{abs}$ values (see Figure S35).[9] The values for **5–6** are typical of organic CPL emitters[2] and nicely illustrate the chiral perturbation induced by the presence of the stereogenic P-atom. It should be noted that, while the $g_{lum}$ values for **5–6** are higher than their non-fused precursors **1–2**, the case is reversed for **3** *vs* **7**, demonstrating the subtlety and complexity of molecular engineering of CPL organic emitters.

In conclusion, eight new π-extended phosphetene rings flanked with PAH systems of various topologies (**1–8**) have been synthesized, and their spectroscopic properties were studied. The presence of an electron-withdrawing P atom (phosphine oxide) generates quasi-reversible electrochemical properties. The P-atom in these systems is stereogenic and the impact of chirality on the optical properties of **1–3** and **5–7** was examined using enantiopure samples obtained through chiral HPLC. In particular, some of these fluorophores showed significant CPL emission induced by the chiral perturbation of the remote stereogenic P-center. Although the flanking four membered rings are not extensively involved in the FMOs (or any other near-lying orbitals), their chiral characters induce asymmetry in the relevant orbitals, resulting in chiroptical properties. Our results indicate that the origin of chirality is not the marginal deviation from planarity, and the dissymmetry of the orbitals is consistent with minor distortions in the aromatic C–C bond lengths, rather than from deviation from planarity. This observation opens many perspectives in the field of organic materials with chiroptical properties, given the diversity of chiral phosphines and P-rings.

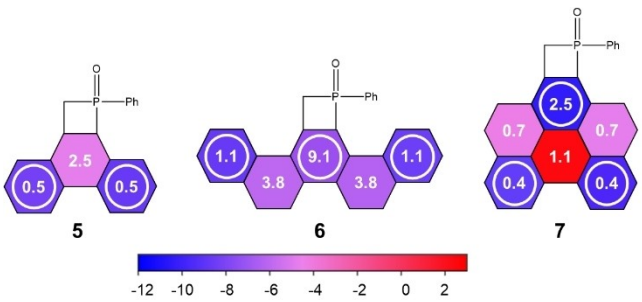


***Figure 8.*** NICS(0)-values (blue to red) at the B3LYP-D3/6-311G**// B3LYP-D3/6-31G* level of theory and the average bond dissymmetry (in $10^{-3}$ Å) at the B3LYP-D3/6-31G* level of theory written inside each ring.

## Experimental Section

Supporting Information include experimental procedures, NMR data, X-ray crystallographic data,[2] photophysical, chromatography and theoretical data.

## Acknowledgements

This work is supported by the MESRI, the CNRS, the Région Bretagne, Campus France, K-147095 of NKFIH, ÚNKP-23-3-I-BME-268, New National Excellence Program, the Doctoral Excellence Fellowship Programme (DCEP), Michael Somogyi program, China-French AIL in "Functional Organophosphorus Materials" and GDR Phosphore. UMS Biosit, Université de Rennes 1 is acknowledged for ECD measurements. Authors warmly thank J. Crassous and L. Favereau (ISCR) for CPL measurements and fruitful discussions.

## Conflict of Interest

The authors declare no conflict of interest.

## Data Availability Statement

The data that support the findings of this study are available from the corresponding author upon reasonable request.

**Keywords:** Polycyclic Aromatic Hydrocarbons · P-heterocycles · 4-member ring · Circularly polarized luminescence

[1] a) M. D. Watson, A. Fechtenkotter, K. Müllen, *Chem. Rev.* **2001**, *101*, 1267–1300; b) J. S. Wu, W. Pisula, K. Müllen, *Chem. Rev.* **2007**, *107*, 718–747.

[2] a) K. Dhbaibi, L. Favereau, J. Crassous *Chem. Rev.* **2019**, *119*, 8846–8953; b) L. Arrico, L. Di Bari, F. Zinna, *Chem. Eur. J.* **2021**, *27*, 2920–2934; c) K. Dhbaibi, L. Favereau, M. Srebro-Hooper, C. Quinton, N. Vanthuyne, L. Arrico, T. Roisnel, B.

Jamoussi, C. Poriel, C. Cabanetos, J. Autschbach, J. Crassous, *Chem. Sci.* **2020**, *11*, 567–576.
[3] a) J. R. Brandt, X. Wang, Y. Yang, A. J. Campbell, M. Fuchter, *J. Am. Chem. Soc.* **2016**, *138*, 9743–9746; b) K. Dhbaibi, L. Abella, S. Meunier-Della-Gatta, T. Roisnel, N. Vanthuyne, B. Jamoussi, G. Pieters, B. Racine, E. Quesnel, J. Autschbach, J. Crassous, L. Favereau, *Chem. Sci.* **2021**, *12*, 5522–5533.
[4] a) E. M. Sanchez-Carnerero, F. Moreno, B. L. Maroto, A. R. Agarrabeitia, M. J. Ortiz, B. G. Vo, G. Muller, S. de La Moya, *J. Am. Chem. Soc.* **2014**, *136*, 3346–3349; b) S. Feuillastre, M. Pauton, L. Gao, A. Desmarchelier, A. J. Riives, D. Prim, D. Tondelier, B. Geffroy, G. Muller, G. Clavier, G. Pieters, *J. Am. Chem. Soc.* **2016**, *138*, 3990–3993.
[5] a) A. Marinetti, J. Fischer, F. Mathey, *J. Am. Chem. Soc.* **1985**, *107*, 5001–5002; b) R. Streubel, H. Wilkens, U. Rohde, A. Ostrowski, J. Jeske, F. Ruthe, P. G. Jones, *Eur. J. Inorg. Chem.* **1999**, 1567–1579; c) L. Dupuis, N. Pirio, P. Meunier, A. Igau, B. Donnadieu, J.-P. Majoral, *Angew. Chem. Int. Ed.* **1997**, *36*, 987–989; d) H. T. G. Walsgrove, B. O. Patrick, D. P. Gates, *Organometallics* **2022**, *41*, 3399–3410; e) T. Xin, C. C. Cummins, *J. Am. Chem. Soc.* **2023**, *48*, 25989–25994; f) Y. Luo, Z. Zhao, T. Chen, Y. Li, Y. Zhao, D. W. Stephan, Y. Wu, *Chem. Commun.* **2023**, *59*, 10956–10959; g) H. Lauwick, M. P. Duffy, P.-A. Bouit, M. Hissler, *Coord. Chem. Rev.* **2021**, *433*, 21375.
[6] a) H. Chen, S. Pascal, Z. Wang, P.-A. Bouit, Z. Wang, Y. Zhang, D. Tondelier, B. Geffroy, R. Réau, F. Mathey, Z. Duan, M. Hissler, *Chem. Eur. J.* **2014**, *20*, 9784–979; b) F. Roesler, M. Kovàcs, C. Bruhn, Z. Kelemen, R. Pietschnig, *Chem. Eur. J.* **2021**, *27*, 9782–9797; lit c > S. Xu, R. Mi, G. Zheng, X. Li, *Chem. Sci. J.* **2024**, *15*, 6012–6021.
[7] K. M. Doxsee, G. S. Shen, *J. Am. Chem. Soc.* **1989**, *111*, 9129–9130.
[8] Chiral separation could not be optimized on **4** and **8**.
[9] H. Tanaka, Y. Inoue, T. Mori, *ChemPhotoChem* **2018**, *2*, 386–402.
[10] For other CPL emitting P-derivatives, see: a) K. Yavari, W. Delaunay, N. De Rycke, T. Reynaldo, P. Aillard, M. Srebro-Hooper, V. Y. Chang, G. Muller, D. Tondelier, B. Geffroy, A. Voituriez, A. Marinetti, M. Hissler, J. Crassous, *Chem. Eur. J.* **2019**, *25*, 5303–5310; b) S. Nishigaki, K. Murayama, Y. Shibata, K. Tanaka, *Mater. Chem. Front.* **2018**, *2*, 585–590; c) R. Mokrai, A. Mocanu, M. P. Duffy, T. Vives, E. Caytan, V. Dorcet, T. Roisnel, L. Nyulászi, Z. Benkő, P.-A. Bouit, M. Hissler, *Chem. Commun.* **2021**, *57*, 7256–7259.
[11] L. Liu, B. Yang, T. J. Katz, M. K. Poindexter, *J. Org. Chem.* **1991**, *56*, 3769–3775.
[12] L. Liu, T. J. Katz, *Tetrahedron Lett.* **1991**, *32*, 6831–6834.
[13] D. Joly, P.-A. Bouit, M. Hissler, *J. Mater. Chem. C.* **2016**, *4*, 3686–3698.
[14] a) J. Trop, M. H. Ihde, A. K. Williams, N. J. White, N. Eedugurala, N. C. Bell, J. D. Azoulay, M. Bonizzoni *Chem. Sci.* **2019**, *10*, 10247–10255; b) S. Fanetti, M. Citroni, R. Bini, L. Malavasi, G. A. Artioli, P. Postorino, *J. Chem. Phys.* **2012**, *137*, 224506.
[15] a) J. R. Platt, *J. Chem. Phys.* **1948**, *17* (5), 484; b) M. Parac, S. Grimme *Chem. Phys.* **2003**, *292*, 11.
[16] For definition and values see Supporting Information under Table S18.
[17] Deposition Numbers 2143473 (for 1), 2143474 (for 2), 2143475 (for 4), 2143477 (for **5**), 2204000 (for (***S***)-**5**), 2143479 (for **6**), 2143480 (for (***S***)-**6**) contain the supplementary crystallographic data for this paper. These data are provided free of charge by the joint Cambridge Crystallographic Data Centre and Fachinformationszentrum Karlsruhe.

Manuscript received: May 27, 2024
Accepted manuscript online: June 27, 2024
Version of record online: September 12, 2024